

Complex Structure of Clusters of Galaxies A1689 and A2218

Karl Andersson (KTH, SLAC), Greg Madejski (SLAC, KIPAC), John Peterson (KIPAC/Stanford), Phil Marshall (KIPAC/Stanford)

Abell 1689

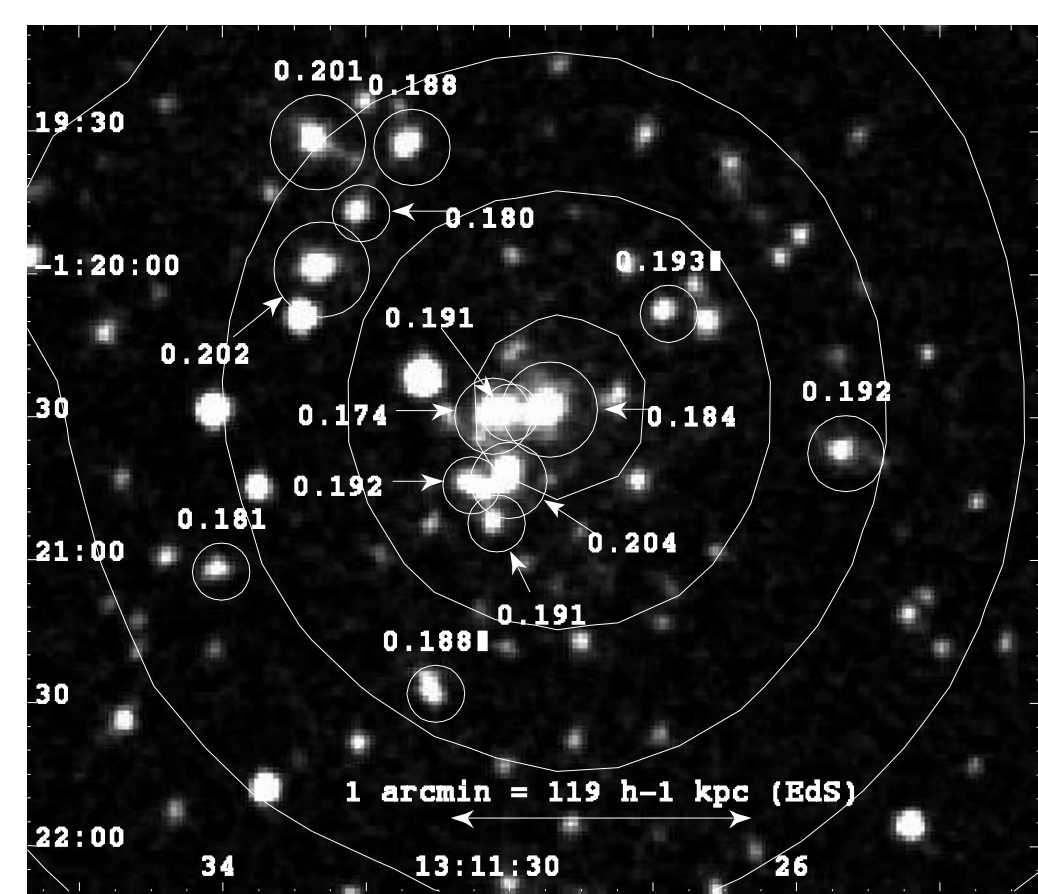


Figure 1: X-ray contours from XMM MOS overlaid R band DSS image. All cluster member within 2' of the cluster centre are encircled. Positions and redshifts are from Duc et al. 2002.

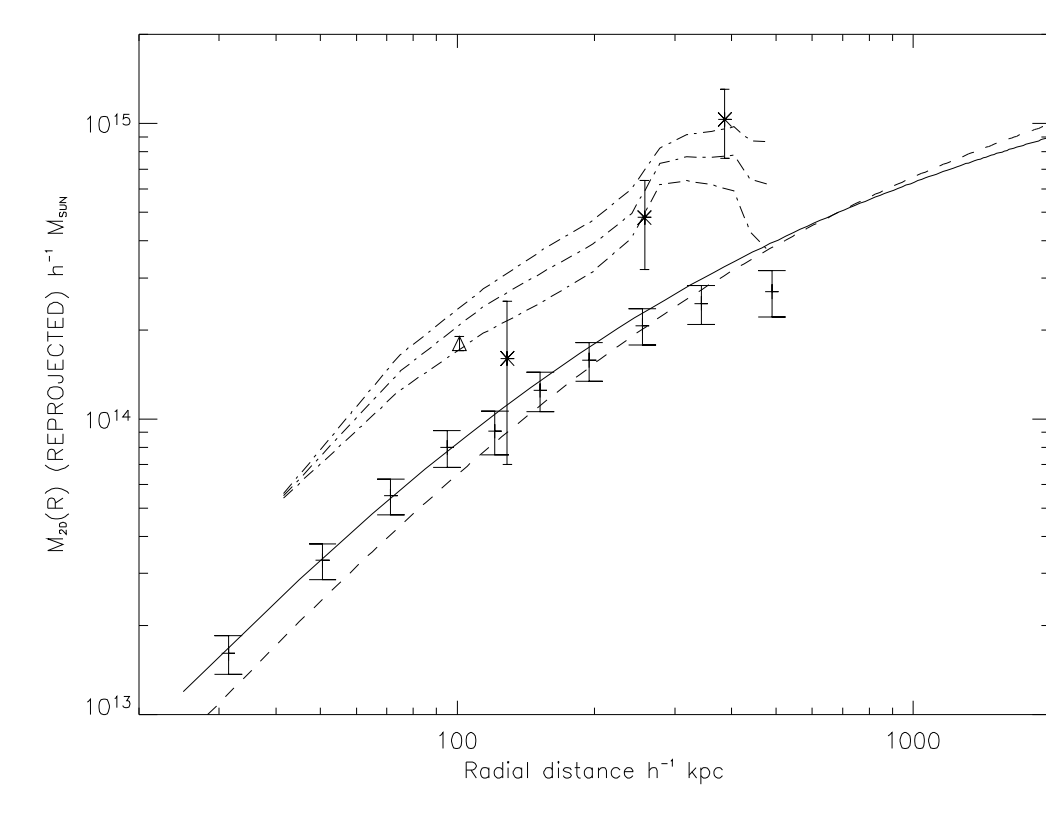


Figure 2: Projected gravitational mass distribution of A1689 calculated using an unparametrized deprojection technique (pluses with 90% CL errors). Reprojected best-fit NFW model (solid line). NFW model from weak gravitational shear analysis (dashed line, Clowe & Schneider (2001)). Strong lensing mass (triangle, Tyson & Fischer (1995)). Weak lensing, distortion of background galaxy luminosity function (asterisks, Dye et al. 2001). Weak lensing, deficit of red background galaxies (dot-dashed lines, Taylor et al. 1998).

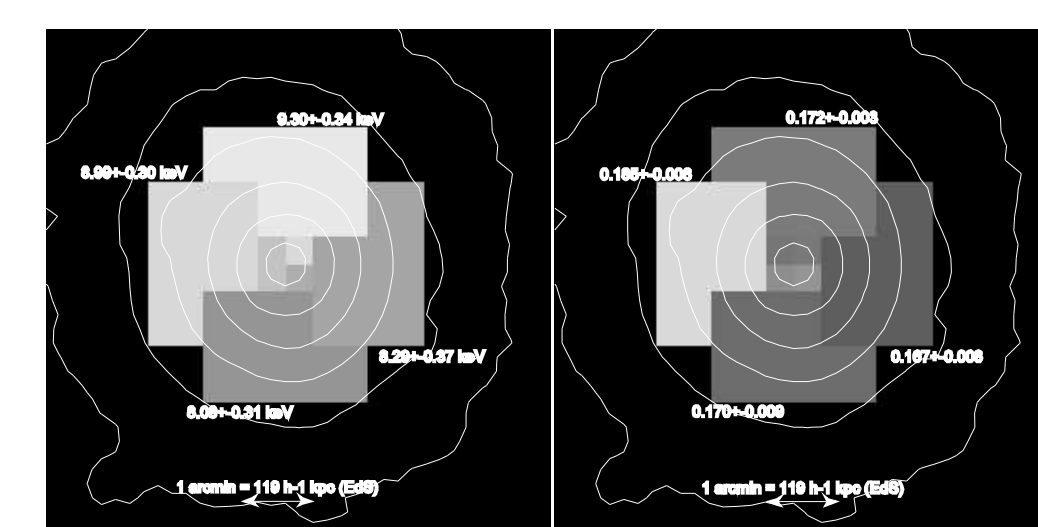


Figure 3: X-ray contours from XMM MOS overlaid temperature map (left) and redshift map (right) of A1689

Abell 1689 is a galaxy cluster at $z = 0.183$ (Teague et al. 1990) well studied by multiple gravitational lensing techniques. We have studied the 40 ks XMM observation of Abell 1689. Comparing the XMM data with data from ROSAT, ASCA and Chandra we verify the XMM low energy response.

We find that the data gives a best fit to a MEKAL model with $kT = 9.00 \pm 0.13$ keV and mean abundances of 0.25 ± 0.02 solar and a redshift of $z = 0.173 \pm 0.003$. The absorbing column is consistent with Galactic.

Using an unparametrized deprojection technique employing spherical symmetry we derive 3-D temperature and gas density profiles. Assuming hydrostatic equilibrium we derive a radial profile of the gravitating mass fitting best an NFW model with concentration $c = 7.7^{+1.6}_{-2.4}$ and virial radius $r_{200} = 1.31 \pm 0.25 h^{-1}$ Mpc (for a $\Omega_m = 0.3$, $\Omega_\Lambda = 0.7$ cosmology).

Comparing with data from various types of gravitational lensing (see Fig. 2 above) we find the X-ray derived mass to be less than half of what most lensing techniques find. We also find a comparably low gas mass fraction of $f_{\text{gas}} = 0.072 \pm 0.008$ at the r_{200} radius.

In analysing the source of the discrepancy we derive temperature and redshift maps for the cluster (Fig. 3 above). The temperature is clearly asymmetric and we find a high-redshift region at $z = 0.185 \pm 0.006$.

The cluster is possibly in the late stages of a merger, this could explain the mass discrepancy.

Abell 2218

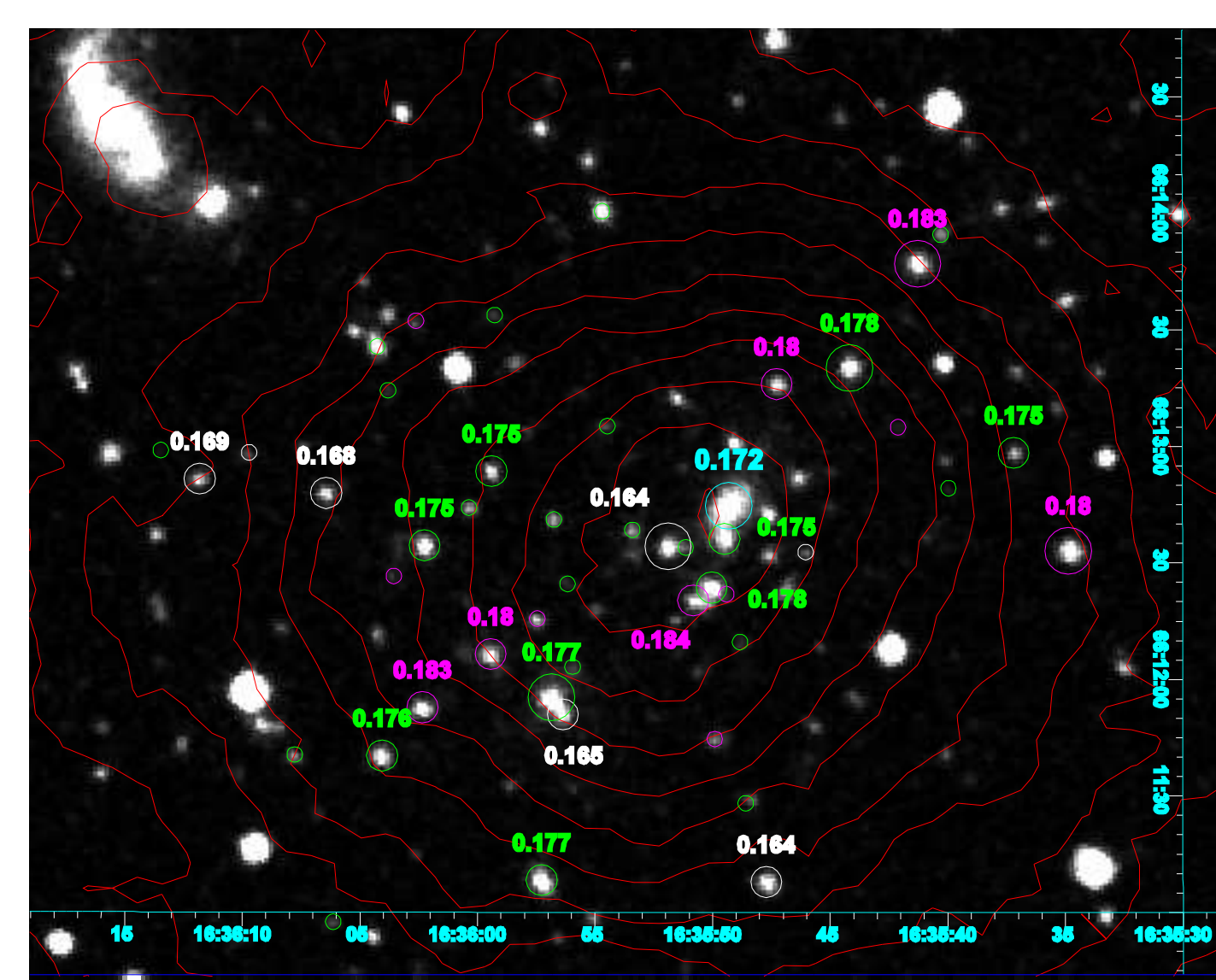


Figure 4: Hard X-ray (2-10 keV) contours from XMM-Newton overlaid DSS red-band image. Positions and redshifts for 48 member galaxies are from LeBorgne et al. 1992. Galaxies with redshifts [$z < 0.17$, $0.17 < z < 0.18$, $z > 0.18$] are marked in [white, green, magenta]. The cD galaxy is marked in cyan. Circle sizes are proportional to r-band magnitudes.

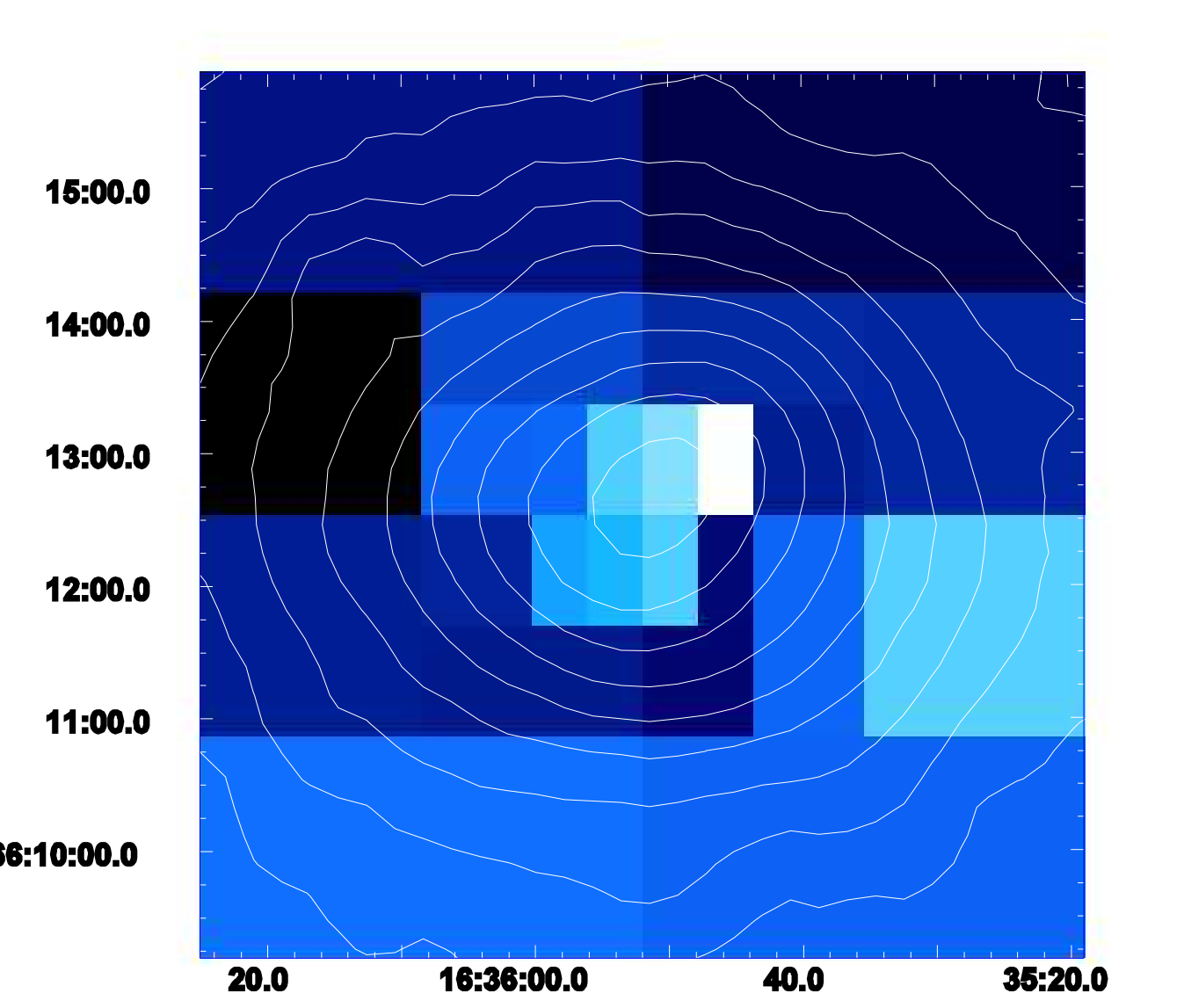


Figure 5: XMM-Newton surface intensity contours overlaid 7' x 7' temperature map employing adaptive binning with minimum 6000 cts/bin.

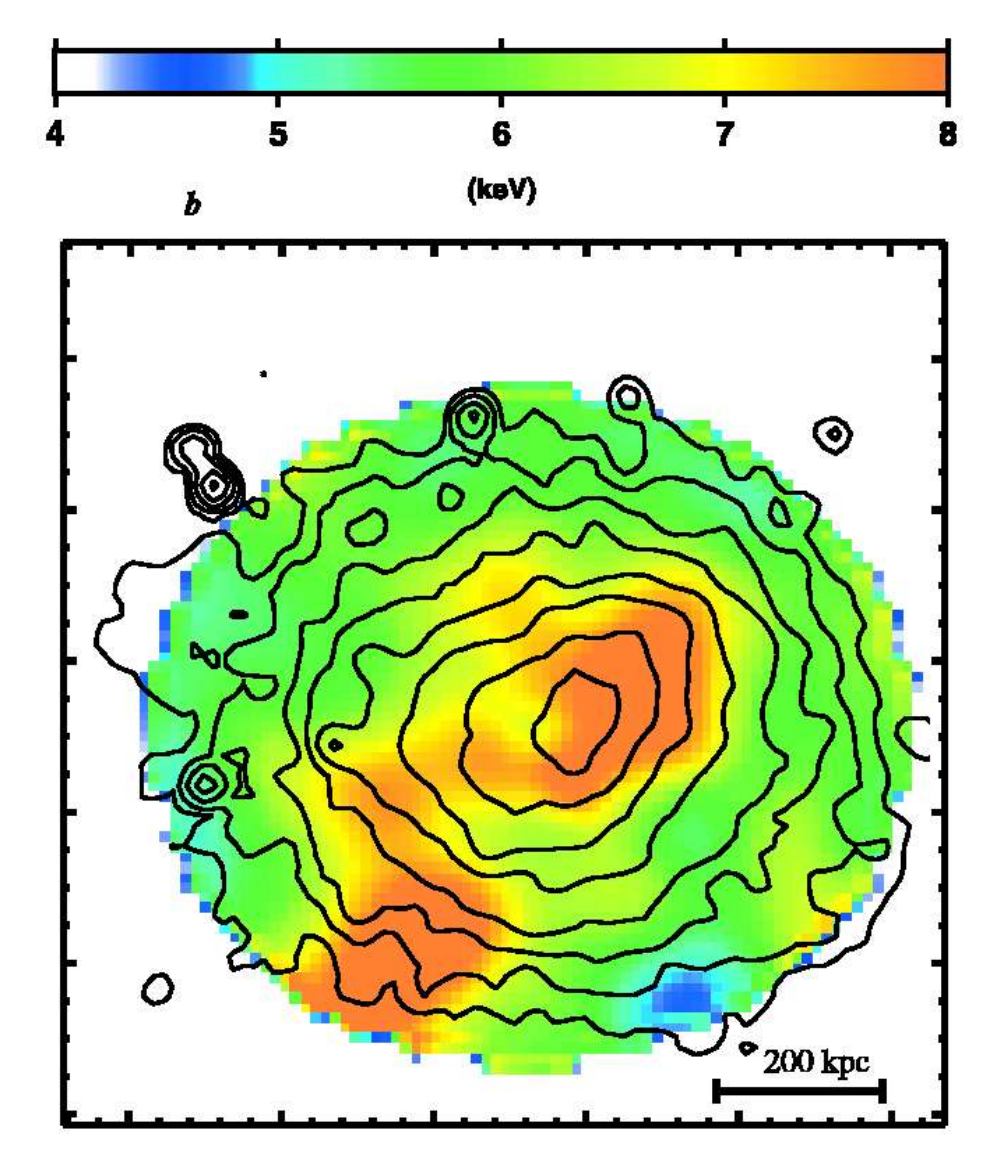


Figure 6: Chandra X-ray contours overlaid temperature map (taken from Govoni et al. (2004) for comparison)

Abell 2218 is a galaxy cluster at $z = 0.17$ where both strong and weak lensing measurements have found two separate peaks in the mass distribution (e.g. Abdelsalam, Saha, & Williams 1998; Kneib et al. 1996). The X-ray temperature map derived from Chandra data (Fig. 6) shows a highly asymmetric structure although the X-ray luminosity is fairly symmetric (Govoni et al. 2004). Machacek et al. (2002) also find two peaks in hard X-ray luminosity (2-7 keV band) separated by $\sim 43''$ in the Chandra data aligned in the NW-SE direction. The soft (0.3-2 keV) X-ray peak is found to be directly in between these hard peaks. Multiple X-ray peaks are also found in ROSAT data (Markevitch 1997).

Here we present the preliminary results of the three, now public, XMM-Newton observations of Abell 2218 taken during the period 2002-09-28 – 2002-10-04. The combined exposure of the observations is ~ 47 ks with all 3 EPIC cameras in use. Spectral analysis of the central 3' region of the cluster suggests $kT = 7.0 \pm 0.2$ keV, metal abundances of 0.20 ± 0.02 Solar in good agreement with previous observations. We also find an average redshift of $z = 0.162 \pm 0.003$. This is significantly lower than the average galaxy redshift of $z = 0.1756$ measured from a spectroscopic survey of 66 cluster galaxies (LeBorgne, Pello, & Sanahuja 1992). The source of this discrepancy is yet to be determined.

Using an adaptive binning technique requiring at least 6000 counts in each spatial bin we make a temperature map of Abell 2218 (Fig. 5) extracting a spectrum for each spatial bin and fitting temperature and abundance separately. The map clearly shows the hot central region ($\sim 8-9$ keV) extending towards the northwest in contrast to the surrounding gas at lower temperature (~ 7 keV). In the central 3'x3' region errors on temperature are ~ 0.5 keV (90% C.L.) whereas in the outer regions the error is ~ 1 keV. The temperature map is in good agreement with the Chandra map (Fig. 6).

To investigate whether the hard X-ray double-peak, seen in the Chandra data, is visible in the XMM-Newton data we combine MOS1 and MOS2 exposures from all observations. The contours (log-scale) from the combined 2-10 keV image are shown in Fig. 4 overlaid on a red-band image from the Digitized Sky Survey. 48 member galaxies with spectroscopic redshifts are plotted as circles with redshifts and positions from LeBorgne et al. 1992. Galaxies with redshifts [$z < 0.17$, $0.17 < z < 0.18$, $z > 0.18$] are plotted in [white, green, magenta]. We do not find any double-peak structure in the XMM image, however this may be due to the limited spatial resolution of XMM. The position of the cD galaxy is offset from the large scale cluster emission centre but roughly at the same position as the highest temperature region in Fig. 5. Instead the centre of X-ray emission is roughly coincident with a giant elliptical galaxy at $z = 0.164$. The line between these galaxies is co-directional with the elongation of the central X-ray emission.

Modelling clusters with an X-ray Monte Carlo (XMC)

Spatial – Spectral modelling of X-ray data using Markov Chain Monte Carlo

Example: Abell 1689

Study of structure of clusters of galaxies in the X-ray band (where one would like to learn about the spatial density and temperature distribution of X-ray emitting gas) is difficult because we observe a 3-D structure projected on the sky

Limited spatial resolution of X-ray mirrors makes this even more challenging

Most current approaches rely on a variety of deprojection techniques, but this is difficult when one uses multiple instruments (e.g. one with good spatial resolution and another with good spectral resolution)

A promising technique, developed for grating spectroscopy of extended sources, might be particularly useful for such an application

The technique which we call "X-ray Monte Carlo" (XMC) provides simultaneous spatial - spectral modeling of X-ray data using a Markov Chain Monte Carlo

The cluster gas is represented by a set of gas clouds ("blobs"), each with its own temperature, density, size, and location

X-rays from such "blobs" are propagated through the instrument, generating trial X-ray data in a form that would be detected by an X-ray telescope/detector

The parameters are iterated using an adaptive Markov chain Monte Carlo method to explore the likelihood distribution of the parameter space

This method lends itself readily for use with multiple instruments simultaneously (First application was to XMM-Newton, but it can be adopted to Chandra and Astro-E2 as well)

The model-independent nature of this method allows in principle the use of lensing and Sunyaev-Zeldovich data in the likelihood optimization, and thus can combine the X-ray/Lensing/SZ for a single multi-approach technique

With this, it should add to our understanding of the physical properties of cluster of galaxies and the process of their formation and their use in cosmological studies

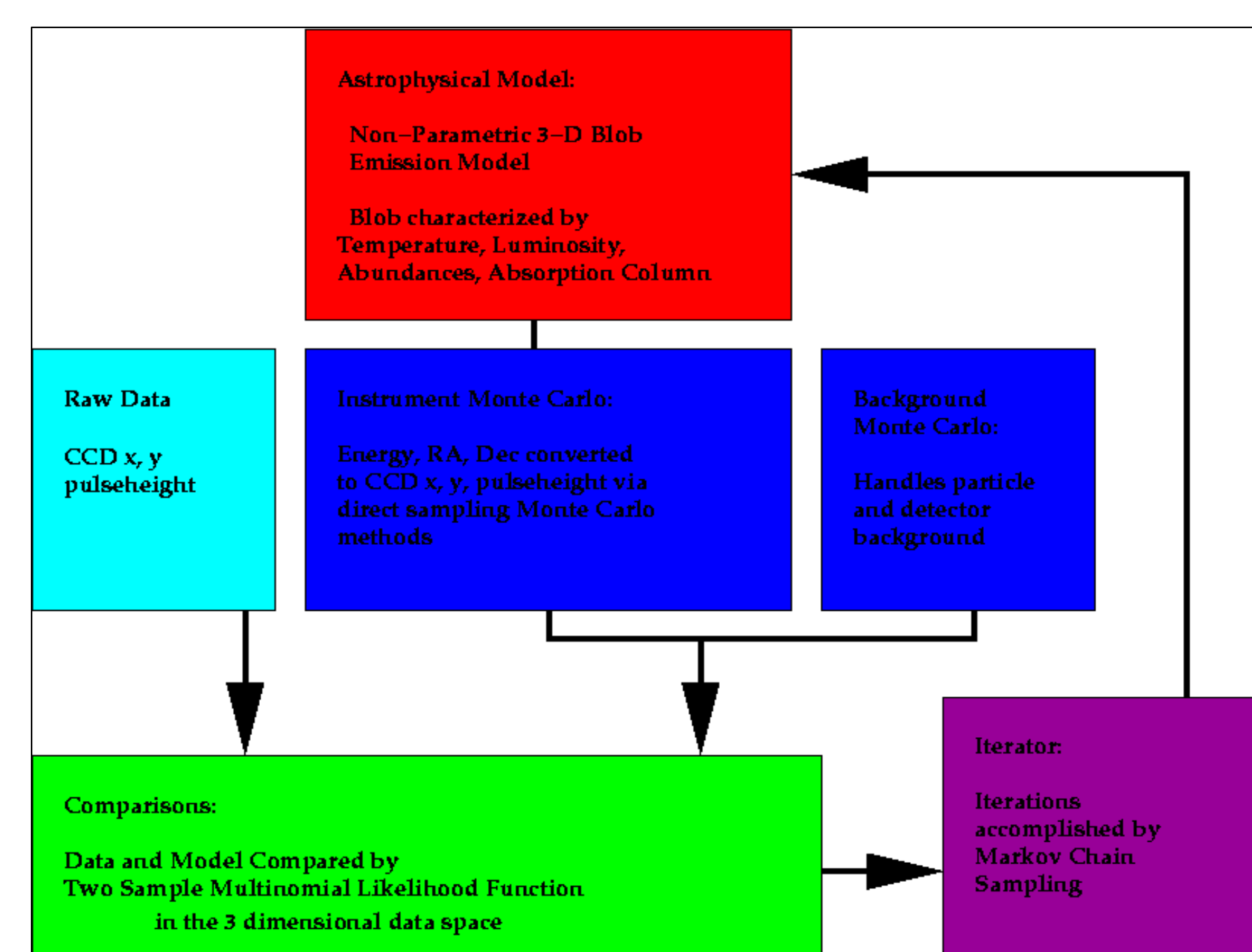


Figure 7: Flowchart of XMC

Basic Method (see flow chart for color coding):

2. Hypothetical "blobs" of plasma are generated; each blob has its own sky position, gaussian width, temperature, luminosity, set of abundances, and absorption column
5. The blob parameters are used to predict photons with sky positions and energies
7. The sky position and energies are used to generate CCD coordinates and pulse heights via direct sampling Monte Carlo methods. These methods use response functions for the X-ray instruments and generate one photon at a time.
9. These simulated events are to be compared with the events from real data
11. The comparison is accomplished by multi-dimensional likelihood statistics
13. The blob parameters are iterated by Markov chain methods
14. The end result is many statistical samples of acceptable fits which can be used to have a "confidence region" of the blob parameters which can describe the plasma

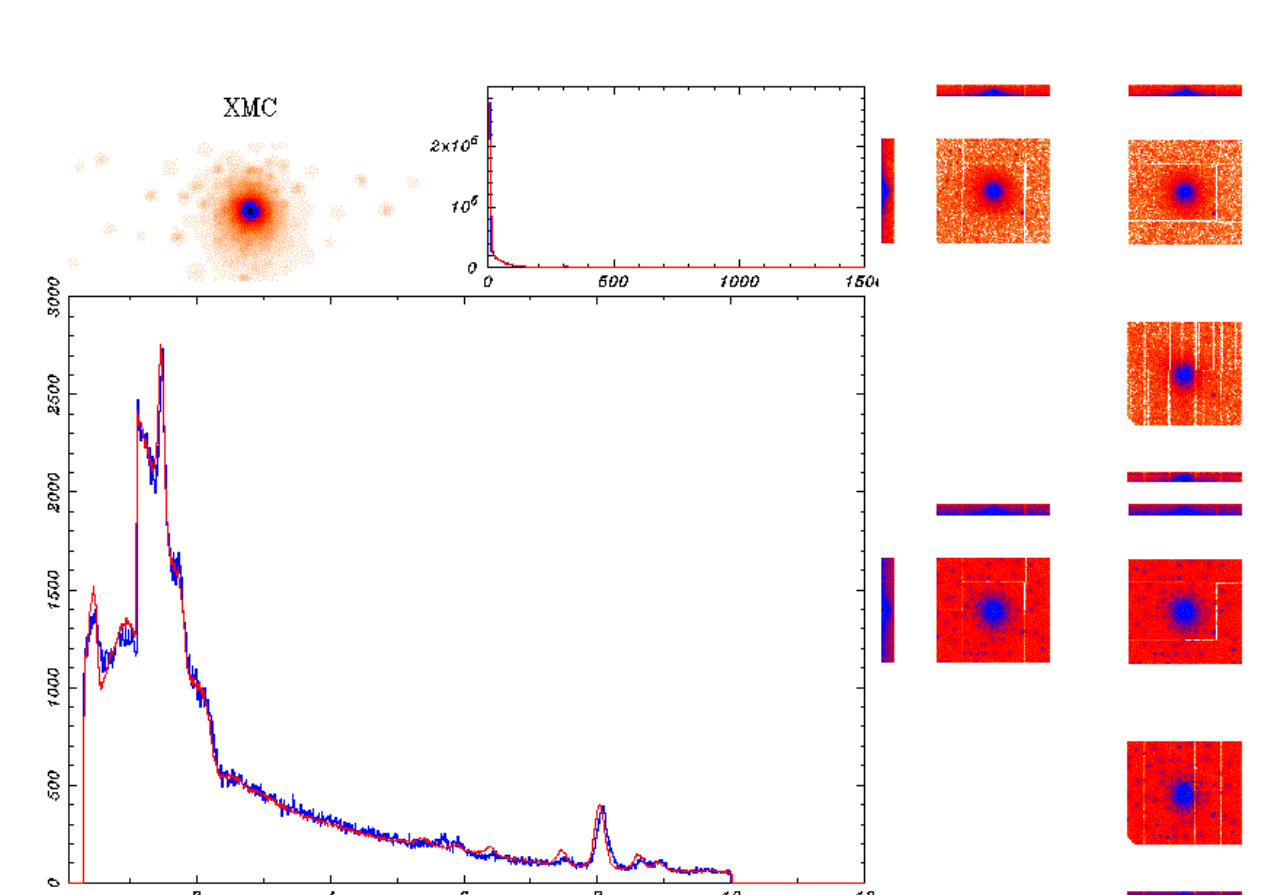


Figure 8: Modelling XMM Abell 1689 observation with XMC. Raw data from the 3 EPIC detectors is shown on 3 top-right plots and the simulated data on the 3 bottom-right plots. The combined spectrum is shown in the bottom-left plot.

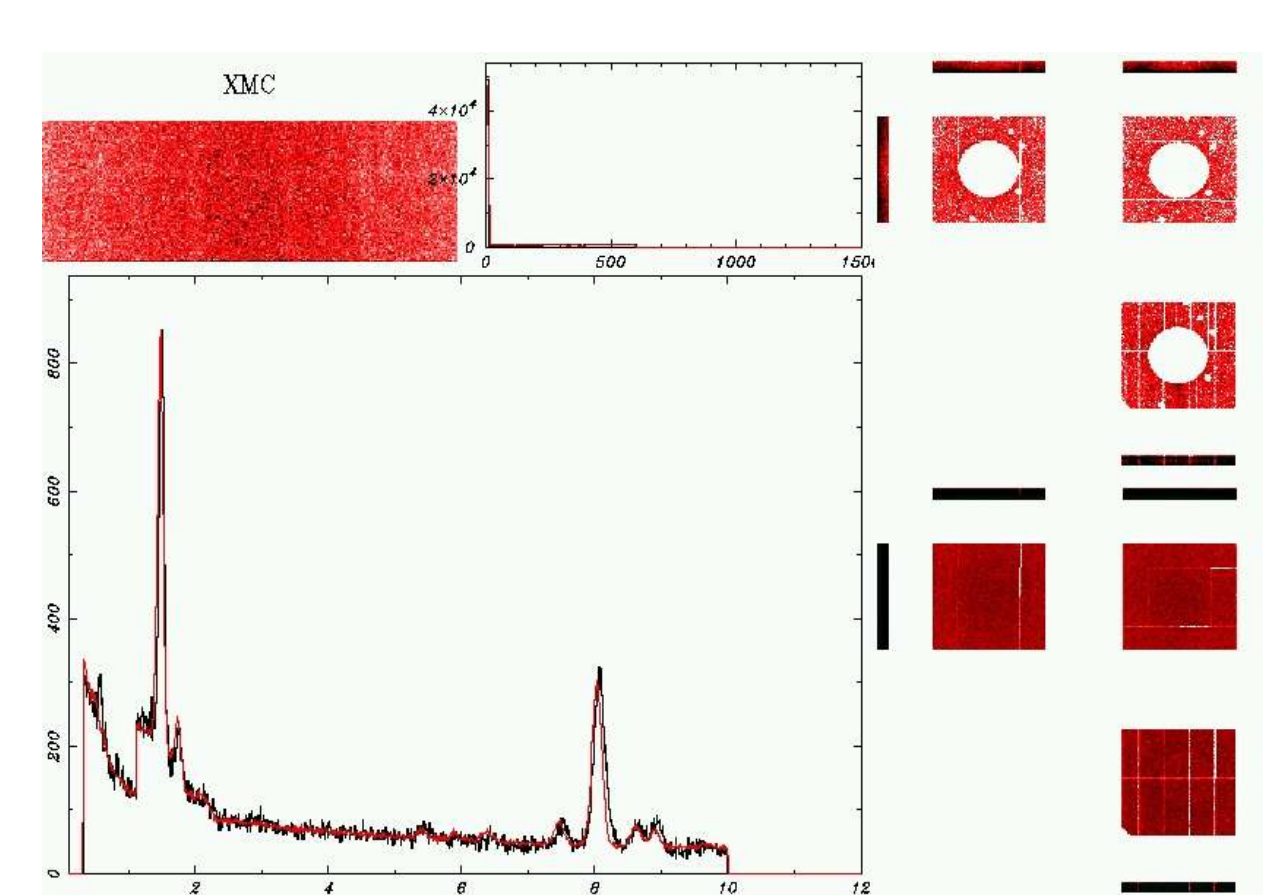


Figure 9: Modelling XMM-EPIC background radiation with XMC. Plots are same as in Fig. 8. The source has been cut out of the data to show the background spectrum alone. Our background model for EPIC includes electronic noise, particles and particle induced emission lines and can be adjusted to give a very good fit (above). The Al-K (1.5 keV) and Cu-K (8 keV) lines are clearly visible.

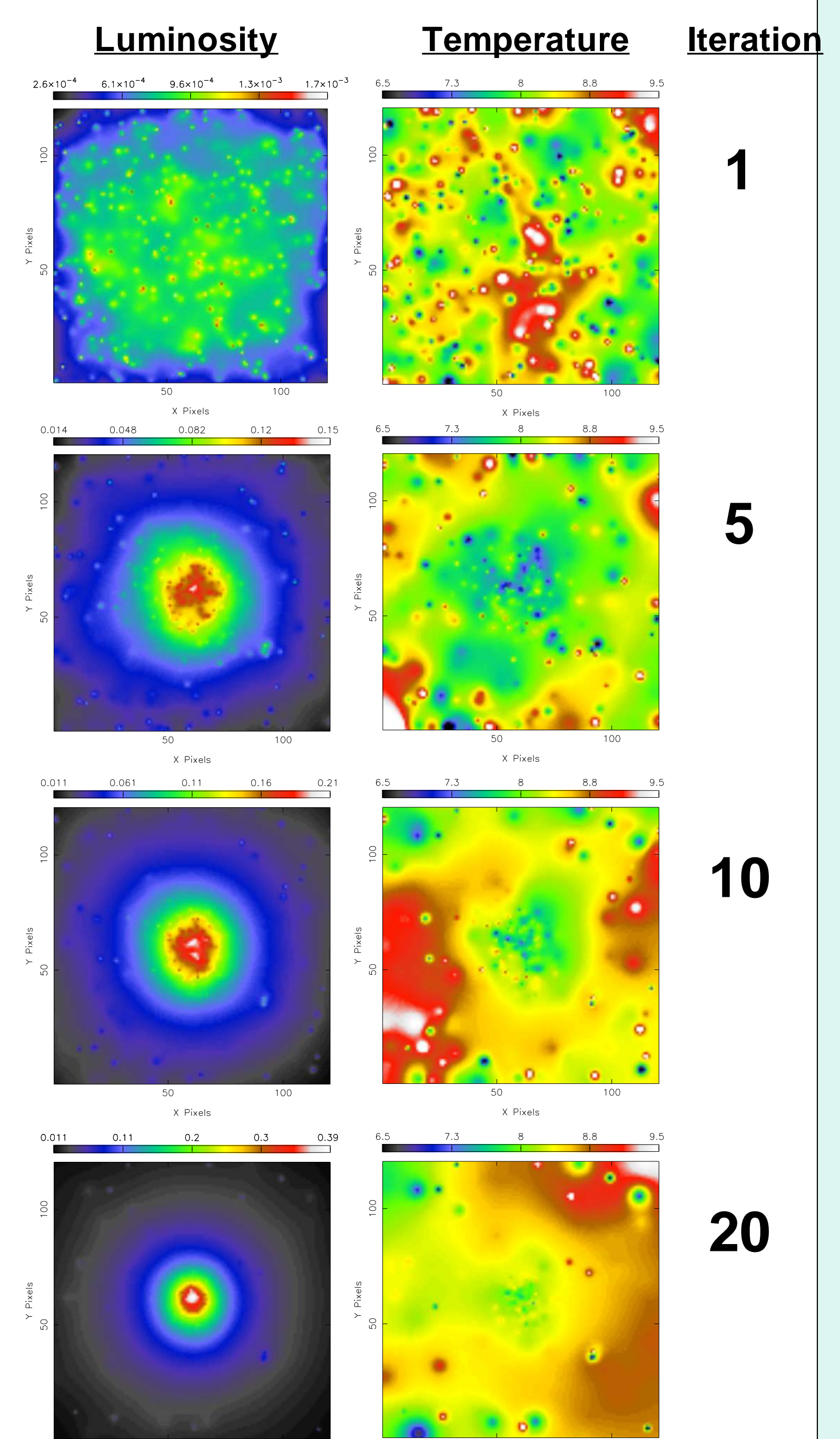


Figure 10: Results of running XMC on the Abell 1689 data. Average luminosity (left) and average temperature in keV (right). Central 10'x10' arcminutes. Note: The simulation has not yet converged.

References:

- AbdelSalam, H. M., Saha, P., & Williams, L. L. R. 1998, AJ, 116, 1541
 Andersson, K. & Madejski, M. 2004, ApJ, 607, 190
 Clowe, D., & Schneider, P. 2001, A&A, 379, 384
 Duc, P. -A. et al. 2002, A&A, 382, 60
 Dye, S., Taylor, A. N., Thommes, E. M., Meisenheimer, K., Wolf, C., & Peacock, J. A. 2001, MNRAS, 321, 685
 Govoni, F., Markevitch, M., Vikhlinin, A., VanSpeybroeck, L., Feretti, L., & Giovannini, G. 2004, ApJ, 605, 695
 Kneib, J. P., Ellis, R. S., Smail, I., Couch, W., & Sharples, R. M. 1996, ApJ, 471, 643
 Le Borgne, J. F., Pello, R., & Sanahuja, B. 1992, A&AS, 95, 87
 Machacek, M. E., Bautz, M. W., Canizares, C., & Garmire, G. P. 2002, ApJ, 567, 188
 Markevitch, M. 1997, ApJ, 483, L17
 Taylor, A. N., Dye, S., Broadhurst, T. J., Benitez, N., & van Kampen, E. 1998, ApJ, 501, 539
 Teague, P. F., Carter, D., & Gray, P. M. 1990, ApJS, 72, 715
 Tyson, J. A., & Fischer, P. 1995, ApJ, 446, L55